ESTIMATES OF P_n AND S_n ACROSS EURASIA

Michael H. Ritzwoller, Mikhail P. Barmin, Anatoli L. Levshin, Antonio Villaseñor, and E. Robert Engdahl

University of Colorado at Boulder

Sponsored by the Defense Threat Reduction Agency
Arms Control Technology Division
Nuclear Treaties Branch

Contract No. DTRA 01-00-C-0013

ABSTRACT

As an intermediate step to producing a integrated P and S model of the crust and upper mantle beneath most of Eurasia to predict regional station specific travel time correction surfaces, we present maps of isotropic P_n and S_n velocities across Eurasia. These maps are constructed using a groomed version of the ISC/NEIC data that are described, in part, by Engdahl et al. (1998). The locations and origin times of the events are replaced with local ground truth locations whenever possible (e.g., Sultanov et al., 1999). We use the tomographic method of Barmin et al. (2000) to estimate P_n and S_n maps on a $1.5^\circ \times 1.5^\circ$ grid, augmented to include station and event static corrections and an epicentral distance or range correction. The starting model is CRUST5.1 (Mooney *et al.*, 1998). We call the P_n and S_n maps together with these corrections the CU P_n/S_n model. Data are used in the inversion if the residual relative to the prediction from the spherical model AK135 (Kennett et al., 1995) is less than 7.5 s for P and 15 s for S, if the event depth is within the crust or less than 50 km deep, if the azimuthal gap to all reporting stations for the event is less than 180 degrees, and if the nominal error ellipse is less than 1000 km^2 in area. We define the phases P_n and S_n as arriving between epicentral distances of 3° and 15°. The resulting data set consists of about $1,600,000$ P_n and $400,000$ S_n travel times inhomogeneously distributed across Eurasia. The P_n and S_n maps compare favorably with recent 3-D models P and S in the uppermost mantle estimated from different data sets (Bijwaard *et al.*, 1998; Villaseñor et al., 2000a) and with recently compiled teleseismic station corrections across the region (Engdahl and Ritzwoller, 2000). The rms misfit to the entire Eurasian data set from the CU P_n/S_n model is 1.8 s for P_n and 3.8 s for S_n. The P_n rms misfit reduces to $\sim$1.7 s for certain high quality subsets of the entire Eurasian data set. We present examples of travel time correction surfaces for several IMS stations or surrogates computed to epicentral distances of 15°. This method will be applied to compute travel time correction surfaces for the remaining IMS stations or surrogates across Eurasia. These correction surfaces will provide an important reference for 3-D models to match and extend.

Key Words: location, Eurasia, P_n, S_n, correction surfaces

OBJECTIVE

The objective of this research is to develop and test a method to produce P_n and S_n station specific travel time correction surfaces across much of Eurasia. This method will be applied systematically to compute correction surfaces for the remaining IMS stations or surrogates across Eurasia to epicentral distances of 15°. These correction surfaces will provide an important reference for emerging 3-D models to match and extend.

RESEARCH ACCOMPLISHED

Introduction

Determination of accurate seismic locations and uncertainties is of prime importance in monitoring the Comprehensive Nuclear Test-Ban Treaty (CTBT). Small magnitude events will only be recorded at a sparse subset of the International Monitoring System (IMS) at regional distances less than 20° - 30°. Sparse network locations are subject to significant bias due to regional variations in the structure of the crust and upper mantle. To meet the goals of the CTBT for these small events, this bias must be substantially reduced in regions of significant structural variability such as that in evidence across much of Eurasia. To do so will require either a model of the 3-D structures or the effects of the structures on the relevant travel-times.

Our ultimate goal is to produce a 3-D P and S model of the crust and uppermost mantle on a $1° \times 1°$ grid beneath N. Africa, the Middle East, and Central Asia that will accurately predict regional travel time variations and improve regional location capabilities. Villaseñor *et al.* (2000a) describe the construction of an S model from surface wave measurements. In order to predict regional S travel times accurately and to convert this model to P, the model will require further calibration using regional body wave travel time data. The study presented here is the first step in this direction. Our approach is not to begin by calibrating the model itself, but rather to calibrate the travel time correction surfaces (e.g., Myers and Schultz, 2000) computed from the model. To do this requires independent estimates of correction surfaces using regional P_n and S_n data. In this paper, we (1) discuss the data set and method used to estimate these correction surfaces, (2) show the first continental scale images of P_n and S_n variations across Eurasia, (3) display the resulting correction surfaces for several IMS surrogate stations, and (4) discuss the fit to the regional phase data.

Data

P_n and S_n travel times are taken from a groomed version of the ISC and NEIC data bases described, in part, by Engdahl *et al.* (1998). ISC travel times are for events that occurred from 1964 through 1997 and NEIC data are from 1998 and 1999. The locations of explosions are replaced with "ground truth" locations whenever possible (e.g., Sultanov et al., 1999). We define the phases P_n and S_n as arriving between epicentral distances of 3° and 15°. At epicentral distances beyond about 10°, however, P_n and S_n may dip into the mantle. The depth of penetration will depend on the radial gradient of velocity, which will vary spatially. Truncation of the data set to include rays only if epicentral distances are less than ∼12°, as in some other studies (e.g., Hearn and James, 1994), severely restricts path coverage in some areas of Eurasia. To utilize longer paths it is desirable to correct for the effect of ray penetration into the uppermost mantle. We discuss the range correction in the next section entitled "Method". This data set totals $3,672,268$ P_n phases and $1,346,676$ S_n phases for $5,418$ stations and 149,929 events worldwide. Data are used in the inversion if the residual relative to the prediction from the spherical model AK135 (Kennett et al., 1995) is less than 7.5 s for P and 15 s for S, if the event depth is within the crust or less than 50 km deep, if the azimuthal gap to all reporting stations for the event is less than 180 degrees, and if the nominal error ellipse is less than 1000 km^2 in area. These selection criteria reduce the data set to $1,636,430$ P_n and $493,734$ S_n phases worldwide. Most of these paths cross Eurasia (0° - 80°N latitude and -10°W - 180°E longitude plus a buffer zone), the numbers being $1,257,052$ for P_n and $422,634$ for S_n.

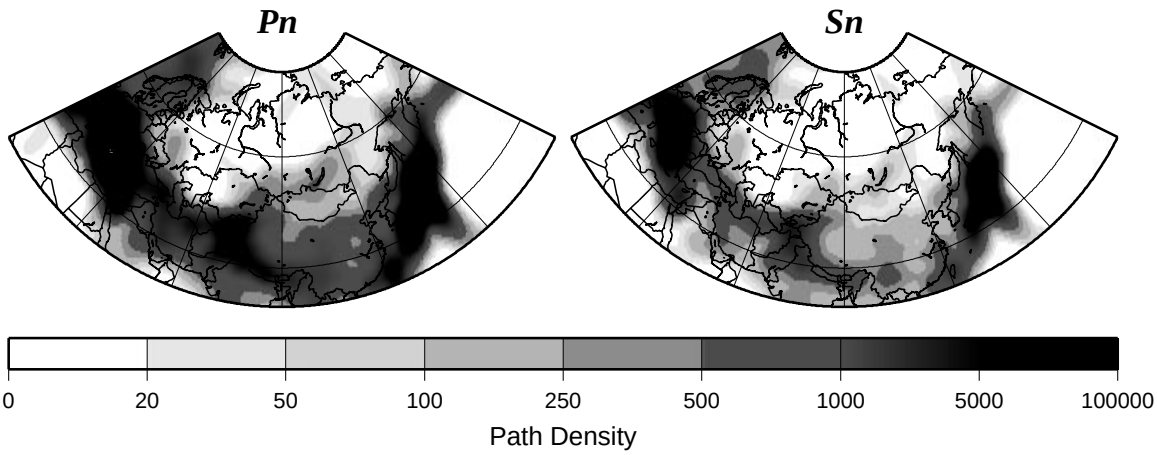

Figure 1: Path density for the P_n and S_n data used here, defined as the number of paths intersecting a $2^\circ \times 2^\circ$ cell ($\sim$50,000km^2). Because path lengths for these phases are by definition short ($< 15^\circ$), paths only exist in regions where both sources and receivers are common. Thus, the path distribution is highly heterogeneous across the region.

Method

The P_n and S_n maps are defined over a two-dimensional surface and, therefore, may be estimated with the same method we developed for surface wave tomography (Barmin *et al.*, 2000). In this method, the model is constructed on an equally spaced grid such that the following figure-of-merit is minimized:

$$(\mathbf{Gm}-\mathbf{d})^T\mathbf{C}^{-1}(\mathbf{Gm}-\mathbf{d}) + \sum_{k=0}^{n}\alpha_k^2||F_k(\mathbf{m})||^2 + \sum_{k=0}^{n}\beta_k^2||H_k(\mathbf{m})||^2, \tag{1}$$

which is a linear combination of data misfit, model roughness, and the amplitude of the perturbation to a reference model. The vector $\mathbf{m}$ represents the estimated model which is a perturbation relative to a reference across the region of interest, $\mathbf{G}$ is the forward operator that computes travel time from the estimated model, $\mathbf{d}$ is the data vector, $\mathbf{C}$ is the data covariance matrix or matrix of data weights, F is a Gaussian smoothing operator, and H is an operator that penalizes the norm of the model in regions of poor path coverage. The spatial smoothing operator is defined over the 2-D model as follows

$$F_k(\mathbf{m}) = m_k(\mathbf{r}) - \int_S S_k(\mathbf{r},\mathbf{r}')m_k(\mathbf{r}')d\mathbf{r}' \ , \tag{2}$$

where S_k is a smoothing kernel:

$$S_k(\mathbf{r},\mathbf{r}') = K_{0k}\exp\left(-\frac{|\mathbf{r}-\mathbf{r}'|^2}{2\sigma_k^2}\right) \tag{3}$$

$$\int_S S_k(\mathbf{r},\mathbf{r}')d\mathbf{r}' = 1, \tag{4}$$

and σ_k is the spatial smoothing width or correlation length. The minimization of the expression in equation (2) explicitly ensures that the estimated model approximates a smoothed version of the model. The maps are estimated on a $1.5^\circ \times 1.5^\circ$ grid across Eurasia.

Barmin *et al.* (2000) discuss tomographic inversions of group and phase velocity data in detail. The inversion for P_n and S_n is essentially the same except that from the reference crustal model we compute source and receiver side Moho penetration points and use these points as the starting and ending points of the ray during inversion. P_n and S_n rays are assumed to be horizontal in a spherical mantle. We have used CRUST5.1 as the reference model in the crust and for P_n and S_n. In addition, we estimate a

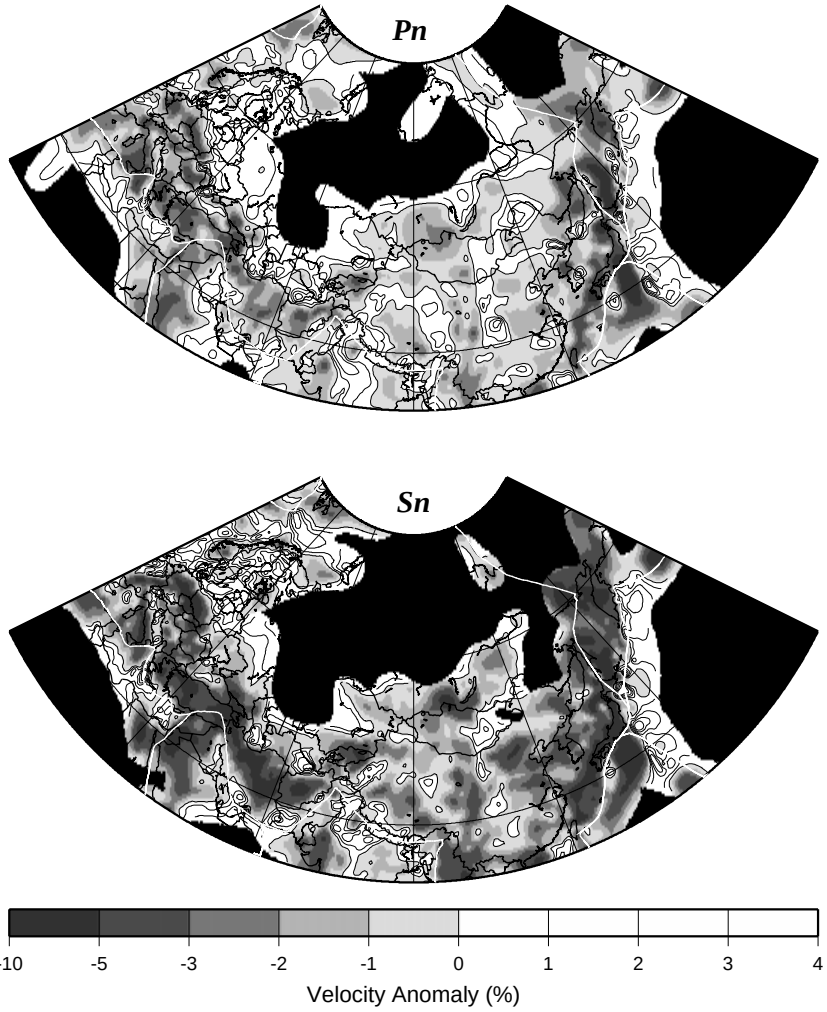

Figure 2: P_n and S_n maps estimated across Eurasia represented as the deviation from the mean across each map in percent. P_n is relative to 8.052 km/s, and S_n is relative to 4.583 km/s. We consider regions in which path density is less than 20 paths/50,000km^2 to be unconstrained by the data, and these regions are shaded black.

range correction and, following Hearn and collaborators (e.g., Hearn and Clayton, 1986; Hearn *et al.*, 1991; Hearn and James, 1994; and elsewhere), we also estimate event and station statics. The range correction is designed to compensate for the fact that rays are not horizontal in the uppermost mantle, but systematically dip further into the mantle as propagation distances increase. This allows us to fit data to greater ranges than is possible without this correction. With this correction, the resulting tomographic maps agree well with those produced with short path data alone (epicentral distances less than 10°) in those regions where tomographic maps can be constructed reliably using only the short path data.

The observed travel time, t_{obs}, is, therefore, modeled as follows:

$$t_{obs} = t_m + t_{crust\_sta} + t_{crust\_evt} + \delta t_{sta} + \delta t_{evt} + \delta t(\Delta) + \int_p \frac{ds}{v_m}, \tag{5}$$

where t_m is the predicted travel time for horizontal rays through the mantle part of the reference model CRUST5.1, the contributions to the travel time due to the reference crustal model CRUST5.1 on the source and event sides are t_{crust_sta} and t_{crust_evt}, the station and event statics are δt_{sta} and δt_{evt}, $\delta t(\Delta)$ is the distance correction, v_m is the estimated velocity at the top of the mantle, and p denotes the appropriate path linking source and receiver through the mantle. Thus, $t_m, t_{crust\_sta}, t_{crust\_evt}$, and p are predicted by the

reference model and $\delta t_{sta}, \delta t_{evt}, \delta t(\Delta)$, and v_m are estimated. A static correction is estimated for a station if there are phase picks from at least 7 events made at that station and an event correction is estimated for all events for which there are at least 20 reporting stations. The asymmetry in this condition is due to the fact that there are more physical phenomena modeled with the event static than with the station static (e.g., mislocation, origin time error). The station and event statics are undamped at present.

We will refer to the P_n and S_n maps together with the corrections $\delta t_{sta}, \delta t_{evt}$, and $\delta t(\Delta)$ as the CU P_n/S_n model to distinguish it from our recent 3-D models (e.g., Villaseñor *et al.*, 2000a).

P_n and S_n Tomography

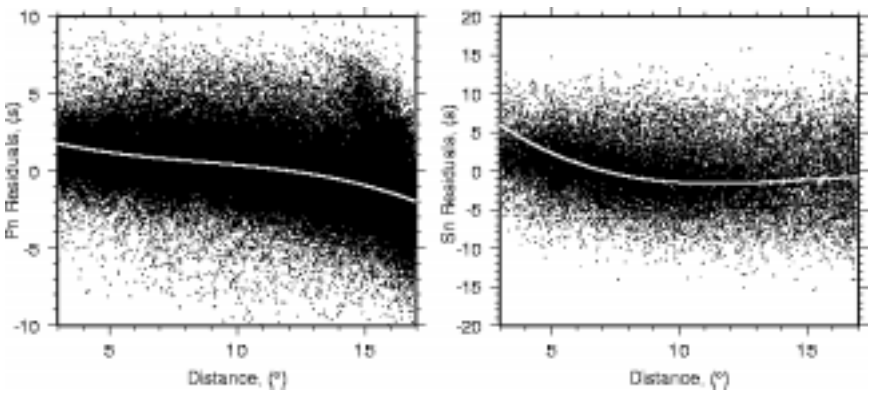

Figure 3: Raw residuals computed for the entire data set using only the P_n and S_n maps shown in Figure 2; these residuals do not include static or range corrections. The white lines are cubic polynomial fits to these data and define the range corrections $\delta t(\Delta)$.

Table 1. Summary of the distribution of station and event statics world-wide.

	P_n		S_n	
static correction	*station (#)*	*event (#)*	*station (#)*	*event (#)*
total	5418	149929	3781	99385
with correction	3295	73587	1780	23737
no correction	2123	76332	2001	75648
max. correction (s)	(-3.78,5.36)	(-6.156,6.89)	(-6.58,10.12)	(-14.56,16.51)
$\# < -2.0$ (s)	4	1396	65	2534
$-2.0 < \# < -1.5$ (s)	14	1884	49	1160
$-1.5 < \# < -1.0$ (s)	57	3781	99	1516
$-2.0 < \# < -0.5$ (s)	177	6801	161	1856
$-0.5 < \# < 0.0$ (s)	580	9890	214	2239
$0.0 < \# < 0.5$ (s)	927	12061	276	2494
$0.5 < \# < 1.0$ (s)	796	12959	231	2358
$1.0 < \# < 1.5$ (s)	425	10913	172	2186
$1.5 < \# < 2.0$ (s)	178	6897	138	1867
$\# > 2.0$ (s)	137	7015	375	5527

The estimated P_n and S_n maps are shown in Figure 2. The velocity anomalies correlate well with known tectonic features and the P_n and S_n maps compare favorably with one another and with the patterns of velocity variations in the 3-D shear velocity model of Villaseñor *et al.* (2000a) and the teleseismic P wave model of Bijwaard and Spakman (1998). Because our tomographic method penalizes the amplitude of the maps in regions of poor data coverage and the estimated maps are perturbations to a reference state, the maps revert to the reference model where data coverage is poor; i.e., less than 15 - 20 paths per each $2^\circ \times 2^\circ$ cell. The areas of poor data coverage are identified as black regions in Figure 2. Both the P_n and S_n maps demonstrate poor coverage across the shield and platform regions of northern Russia and Kazakhstan, in the

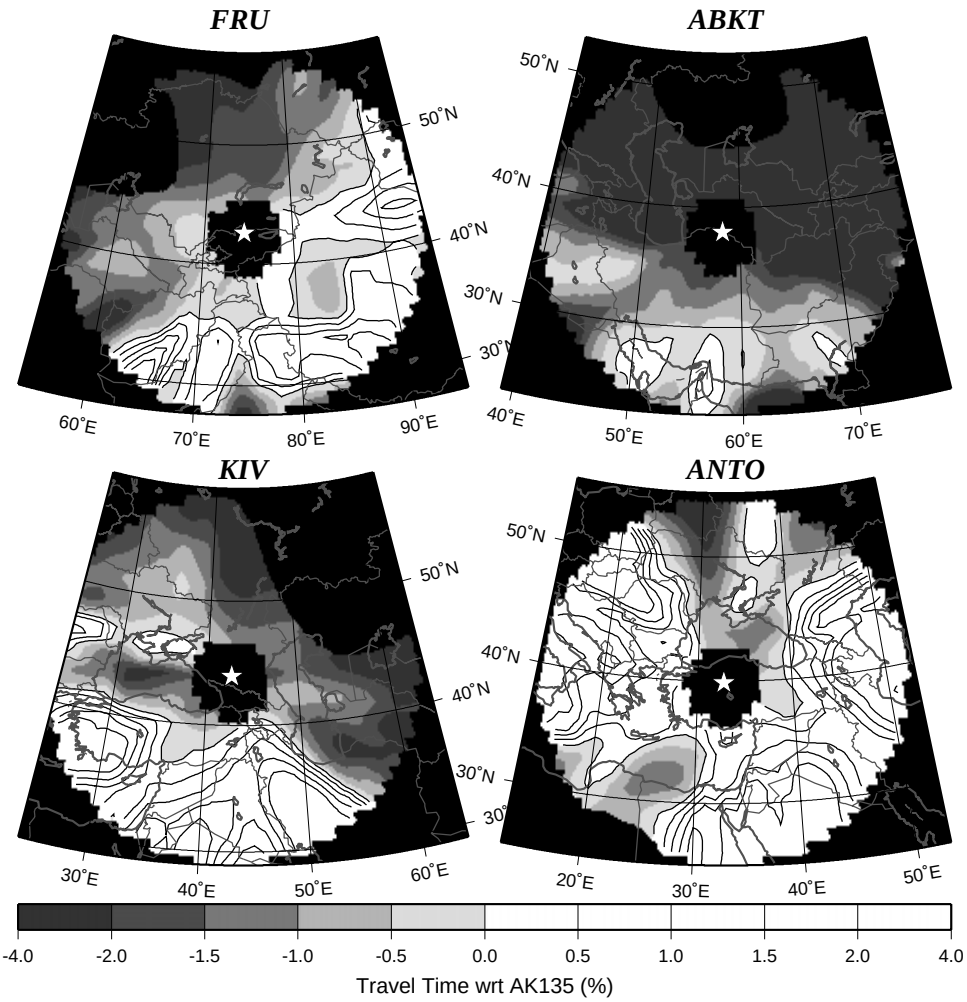

Figure 4: Station specific travel time correction surfaces for P_n for four IMS stations or surrogates (FRU $\rightarrow$ AAK, ANTO $\rightarrow$ BRAR, KIV $\rightarrow$ KBZ). Surfaces exist only where P_n data density is locally greater than 20 paths per 50,000 km^2 and to 15° from the station. Low data density regions are shaded black.

oceans, and across North Africa. Elsewhere the spatial resolution of the maps is estimated to be between 150 - 300 km.

The range correction is shown in Figure 3. This figure shows that mispicks from the triplication from the 400 km discontinuity begin to emerge in the data set at about 15°, which is the reason we have limited the P_n and S_n maps to this distance. The number of S_n picks reduces sharply after about 10°. Station and event statics, δ_{sta} and δ_{evt}, are summarized in Table 1 for the entire data set world-wide. Although for P_n we estimate static corrections only for about 60% of the stations and half of the events world-wide and for S_n the numbers are about 50% and 25%, respectively, the great majority of the measurements emanate from events and are recorded at stations that have static corrections. This is particularly true for P_n, where only 3% of the measurements are made at stations without static corrections and 12% of the measurements are for events without event corrections. For S_n, the numbers are 4% and 33%, respectively. Thus, most measurements have the full complement of corrections applied. Not surprisingly, statics for S_n are typically larger than for P_n and event statics are larger than station statics. This is because S variations in the crust and upper mantle are typically larger than P by about a factor of two and, in addition to compensating for errors in the crustal model, event statics also compensate for mislocations and origin time errors. Event statics also are more effective at reducing rms misfit. Although not shown here, the P_n and S_n station statics are geographically coherent and correlate with one another with a poorly determined S/P ratio of about 1.8.

However, because the statics are determined simultaneously their values are interdependent and difficult to interpret in abstraction from the others. In addition, because we have not constrained the values of the static corrections, in some cases they are probably too large in magnitude, particularly S_n event statics.

Figure 4 displays station specific travel time correction surfaces for several IMS stations or surrogates. These surfaces are for surface sources with the local elevation observed at the station elevation. This differs from correction surfaces as they are commonly displayed in which both the source and station are on the reference ellipsoid. The correction surface for ANTO (Ankara, Turkey) compares favorably with the surfaces from two nearby stations in Turkey (KAS, KVT) reported by Myers and Schultz (2000) using a different method.

Fit to the Data

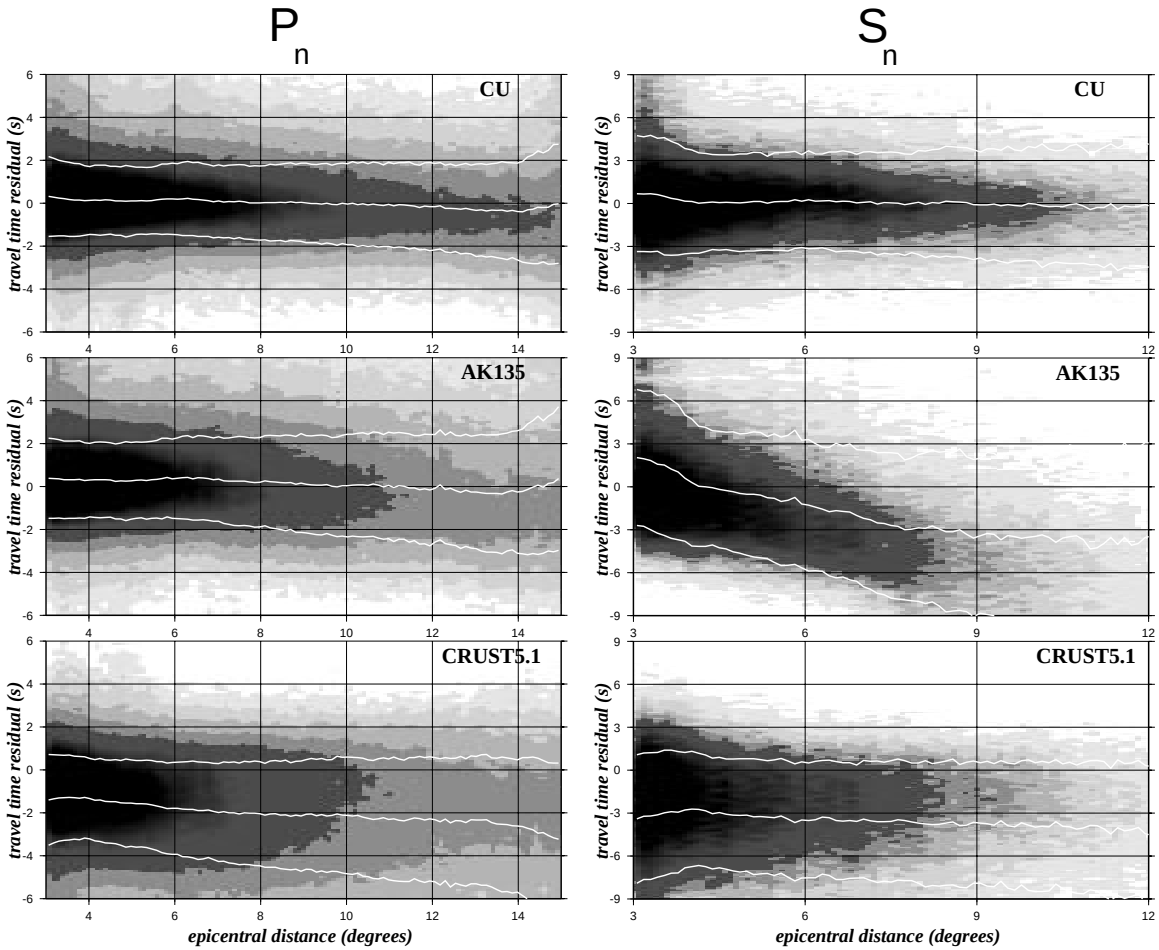

Figure 5: Shaded plots of the density of P_n and S_n travel time residuals (observed - predicted) for the Eurasian data set presented versus epicentral distance. Results for three models are shown: (TOP) the CU P_n/S_n model, (MIDDLE) the spherically symmetric model AK135 (Kennett *et al.*, 1995), and (BOTTOM) the laterally heterogeneous crustal, P_n, and S_n model CRUST5.1 (Mooney *et al.*,1998). Darker shades indicate larger number of residuals and the white lines show the local mean and $\pm 1\sigma$. Means and standard deviations are summarized in Table 2.

Table 2. Summary of misfits to the whole Eurasian data set displayed in Figure 5.

	P_n		S_n	
model	*mean (s)*	σ *(s)*	*mean (s)*	σ *(s)*
CU P_n/S_n	0.06	1.81	0.12	3.83
AK135	0.23	2.06	-0.94	5.36
CRUST5.1	-1.80	2.37	-4.03	5.14

Misfits to the entire Eurasian data set for P_n and S_n are shown in Figure 5 and summary statistics are presented in Table 2. The standard deviation σ reported in Table 2 is computed relative to the mean, so total rms misfit must incorporate the mean. In general, short distance offsets result from errors in the crustal model either in average crustal velocities or Moho depths. Errors in the uppermost mantle velocities manifest themselves as trends with distance. The model AK135 does very well for P. Improvements afforded by the CU P_n/S_n model over AK135 on average begin only after about 8°. However, on average, for both P and S CRUST5.1 is too slow in the crust whereas AK135 is fine for P but too fast for S. CRUST5.1 displays only weak distance trends which indicates that the average upper mantle velocities are reasonable, but AK135 is too slow for S_n, demonstrating a very strong trend. This indicates that uppermost mantle S velocities in AK135 are too slow on average for Eurasia or the depth gradient in the uppermost mantle is not right. The overall rms misfit from our inversions is 1.8 s across all of Eurasia for P_n and approximately twice this value for S_n. These misfit statistics appear to be consistent with those reported by Myers and Schultz (2000) in a study limited to the neighborhood of the Racha earthquake sequence (Caucasus Mountains).

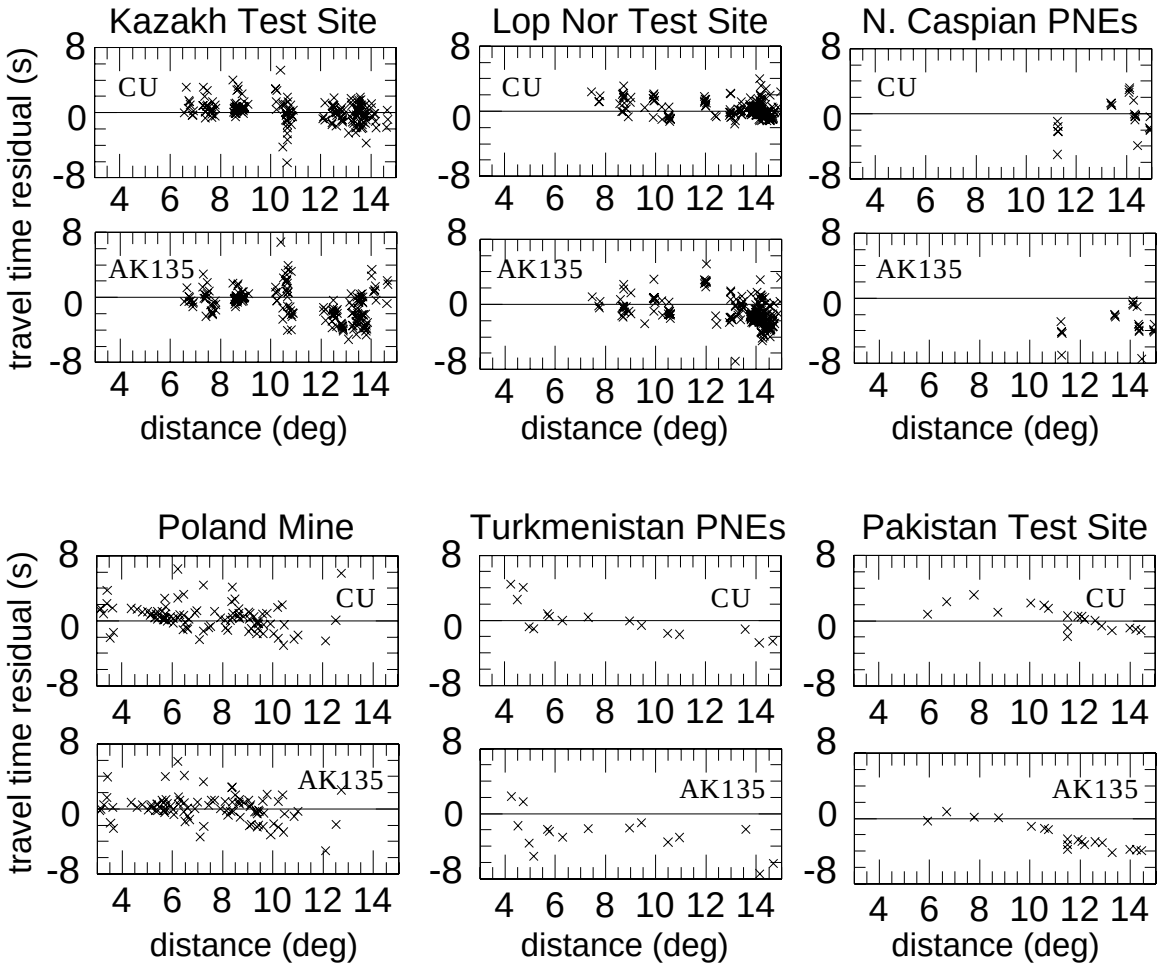

Figure 6: Misfits to P_n and S_n measurements from selected explosions that occurred at six source locations. The upper of each pair of plots for each source location is for the CU P_n/S_n model and the lower of each pair is for the model AK135 Summary statistics are presented in Table 3.

The entire Eurasian data set is very noisy and many locations and origin times are poorly known. A better estimate of expected misfit may come from explosion data in which in many cases the epicenter is well constrained, although the origin times may not be. Figure 6 displays misfits to data from six explosion regions (3 test sites, 2 PNE locations, and 1 large mine) and Table 3 summarizes these data. Only explosions with $m_b \geq 4.6$ as reported in the PDE are used. With the exception of the large mine explosion in south-

western Poland, these events are not observed at enough stations with regional phases to have event statics. The overall misfit of the CU P_n/S_n model to these explosion data is 1.68 s for P_n, which is slightly reduced over the entire Eurasian data set. For events at the three test sites, however, misfit is better than 1.45 s for P and the fit afforded by AK135 is considerably worse. Again, most of the improvement over AK135 delivered by the CU P_n/S_n model comes for paths longer than about 8°. A similar rms misfit of 1.7 s results from a subset of the complete Eurasian data set that consists only of events with $m_b \geq 4.6$ and measurements from events with an event correction measured at stations with a station correction.

Table 3. Summary of misfits to explosion data for P_n displayed in Figure 6.

				rms misfit (s)	
Location	# meas.	# stations	# events	CU P_n/S_n	AK135
Kazakh Test Site	189	18	42	1.38	2.08
Lop Nor Test Site	204	39	19	1.16	1.90
N. Caspian PNEs	22	7	6	2.10	3.72
Pakistan Test Site	19	18	2	1.43	2.72
Poland Mine	92	92	1	1.72	1.68
Turkmenistan PNEs	16	16	1	2.04	3.45
Total	542	-	-	1.68	2.71

CONCLUSIONS AND RECOMMENDATIONS

Conclusions

The method for producing P_n and S_n maps with associated parametric corrections appears to effectively summarize the information in the large groomed ISC/NEIC data base. The P_n and S_n maps correlate well with other high resolution information about structural variations in the uppermost mantle. The station specific travel time correction surfaces computed from the CU P_n/S_n model appear to be robust and fit the data with very low levels of bias at epicentral distances from 3° to 15°. Overall rms misfits across Eurasia for P_n are ~1.8 s and for S_n ~3.8 s and are better for data subsets chosen for their quality (e.g., explosions, large magnitude events, independent information about epicenter location and/or origin time). These misfits are considerably better than those produced by AK135 and CRUST5.1. The correction surfaces will provide an important reference for 3-D models to match and extend.

Recommendations

- **Continued development of the method.** Small modifications to the method may continue to improve the results. For example, although a better starting model of the mantle will not appreciably change the estimated P_n and S_n maps it may help to stablize the static corrections and the range correction. Also, the range correction, which exists to compensate for ray penetration into the mantle, may be improved if it depended on tectonic region because vertical gradients probably vary between tectonic regions.
- **Systematic application of this method to compute station specific travel time correction surfaces across Eurasia.** The method should be applied systematically across all of Eurasia to all IMS stations and surrogates as a reference for future studies.
- **Use of these correction surfaces to calibrate the correction surfaces computed from emerging 3-D models.** The computation of correction surfaces from 3-D models is technically straightforward (e.g., Villaseñor *et al.*, 2000b), but there are practical problems. For example, there are few constraints on variations in crustal velocities across most of Eurasia and the mantle model is probably more accurate in S than in P. Thus, raw predictions from existing models such as that of Villaseñor *et al.* (2000a) are not likely to be as accurate as desired. The correction surfaces shown here will help to calibrate the surfaces computed from 3-D models.

REFERENCES

Barmin, M.P., M.H. Ritzwoller, and A.L. Levshin, A fast and reliable method for surface wave tomography, *Pure and Appl. Geophys.*, in press, 2000.

Bijwaard, H., W. Spakman, and E.R. Engdahl, Closing the gap between regional and global travel time tomography. *J. Geophys. Res.*, **13**, 30055-30078, 1998.

Engdahl, E.R. and M.H. Ritzwoller, Crust and upper mantle P- and S-Wave delay times at Eurasian seismic stations, *Phys. Earth. Planet. Int.*, submitted, 2000.

Engdahl, E.R., R. van der Hilst, and R. Buland, Global teleseismic earthquake relocation with improved travel time and procedures for depth determination, *Bull. Seism. Soc. Am.*, **88**, 722 - 743, 1998.

Hearn, T., N. Beghoul, and M. Barazangi, Tomography of the Western United States from regional arrival times, *J. Geophys. Res.*, **96**, 16369 - 16381, 1991.

Hearn, T.M. and R.W. Clayton, Lateral velocity variations in Souther California. I. Results for the upper crust from P_g waves, *Bull. Seismc. Soc. Am.*, **76**, 495-509, 1986.

Hearn, T.M. and F.N. James, Pn velocities beneath continental collision zones: the Turkish-Iranian plateau, *Geophys. J. Int.*, **117**, 273-283, 1994.

Kennett, B.L.N., E.R. Engdahl, and R.Buland, Constraints on seismic velocities in the Earth from travel times, *Geophys. J. Int.*, **122**, 108-124, 1995.

Mooney, W.D., G. Laske, and G. Masters, CRUST 5.1: A global crustal model at 5 degrees by 5 degrees, *J. Geophys. Res.*, **103**, 727 - 748, 1998.

Myers, S.C. and C.A. Schultz, Improving sparse network seismic location with Bayesian kriging and teleseismically constrained calibration events, *Bull. Seism. Soc. Am.*, **90**, 199 - 211, 2000.

Sultanov, D.D., J.R. Murphy and Kh.D. Rubinstein, A seismic source summary for Soviet peaceful nuclear explosions, *Bull Seism. Soc. Am.*, **89**, 640-647, 1999.

Villaseñor, A., M.H. Ritzwoller, A.L. Levshin, M.P. Barmin, E.R. Engdahl, W. Spakman, and J. Trampert, Shear velocity structure of Central Eurasia from inversion of surface wave velocities, *Phys. Earth Planet. Int.*, submitted, 2000a.

Villaseñor, A., M.H. Ritzwoller, M.P. Barmin, E.R. Engdahl, and A.L. Levshin, Computation of travel times and station correction surfaces in Eurasia using three-dimensional velocity models, this volume, 2000b.